CLIMATOLOGY

Reconciling atmospheric CO_2, weathering, and calcite compensation depth across the Cenozoic

Nemanja Komar* and Richard E. Zeebe

The Cenozoic era (66 to 0 million years) is marked by long-term aberrations in carbon cycling and large climatic shifts, some of which challenge the current understanding of carbon cycle dynamics. Here, we investigate possible mechanisms responsible for the observed long-term trends by using a novel approach that features a full-fledged ocean carbonate chemistry model. Using a compilation of pCO_2, pH, and calcite compensation depth (CCD) observational evidence and a suite of simulations, we reconcile long-term Cenozoic climate and CCD trends. We show that the CCD response was decoupled from changes in silicate and carbonate weathering rates, challenging the continental uplift hypothesis. The two dominant mechanisms for decoupling are shelf-basin carbonate burial fractionation combined with proliferation of pelagic calcifiers. The temperature effect on remineralization rates of marine organic matter also plays a critical role in controlling the carbon cycle dynamics, especially during the warmer periods of the Cenozoic.

INTRODUCTION

Global climate and the global carbon cycle have undergone substantial changes since the Early Eocene [~50 million years (Ma)], the period of peak Cenozoic deep ocean temperatures (*1*–*3*). Warming dominated during the Paleocene (~58 Ma), and the average temperature was steadily rising (high-latitude surface and deep ocean warmed by ~4°C) until it reached its maximum around 6 Ma later (Fig. 1A) (*1*, *2*), as inferred by a negative excursion in stable oxygen isotope ratios ($\delta^{18}O$). The temperature increase during the Late Paleocene and Early Eocene (LPEE; 58 to 52 Ma) was accompanied by a long-term decrease in stable carbon isotope ratios ($\delta^{13}C$) in both surface and deep ocean (Fig. 1B), indicating a drop in the net organic carbon output from the ocean and atmosphere and reordering in carbon cycling (*4*, *5*). Concomitant with the temperature rise was a global deepening of the calcite compensation depth (CCD) of at least 500 m (*4*, *5*).

Since the Cenozoic temperature maximum, the Earth system has experienced gradual cooling, which eventually resulted in major glaciation and ice cap formation at high latitudes, as reflected in $\delta^{18}O$ (*1*, *3*). Evidence suggests that the primary cause of the long-term cooling was a decreasing concentration of atmospheric CO_2 (Fig. 1C) (*6*, *7*). However, the reason behind the CO_2 decline remains enigmatic as some studies suggest a generally constant CO_2 degassing rate over the same time period while others suggest a decrease (*8*–*10*). Lower CO_2 concentrations in the atmosphere result in colder temperatures and a weakened hydrological cycle, which led to decelerated weathering rates lowering ocean alkalinity (and carbonate saturation). This ultimately induces shoaling of the carbonate compensation depth. The CCD is often operationally defined as the depth at which sediments bear less than 5 or 10 weight % $CaCO_3$ (*11*), and as such, its evolution (temporal and spatial) can be traced over the geologic past by inspecting the $CaCO_3$ content of the sediment cores (*12*–*14*).

Contrary to expectations, however, the deep-sea carbonate records indicate that the Pacific CCD deepened over 1 km, from ~3.0 to 3.5 km in the earliest Eocene to about 4.6 km at present (*12*, *13*), creating a carbon cycle conundrum. Similar trends are also observed in the Atlantic and Indian basins (Fig. 1D). As the carbonate preservation in the sediments is mostly a function of the carbonate saturation state of the ocean, the position of the CCD reflects changes in carbonate saturation (*11*), which is, in turn, controlled by the balance between sinks and sources of carbon, which govern atmospheric CO_2. Thus, the variable position of the paleo-CCD over time carries a signal of the combined carbon cycle dynamics of the past. Tracing the CCD evolution across the Cenozoic and identifying mechanisms responsible for its fluctuations are therefore important in deconvolving past changes in atmospheric CO_2, weathering, and deep-sea carbonate burial (*5*).

Here, we present the first modeling study that investigates carbon cycling across the Cenozoic with a full-fledged ocean carbonate chemistry model and predictive organic carbon burial that also incorporates a marine sediment component, crucial for the CCD reconstruction. We use an expanded version of the LOSCAR model [Long-term Ocean-Atmosphere Sediment CArbon cycle Reservoir; (*15*)], called LOSCAR-P, which combines the long-term phosphorus (P) and carbon cycle (*16*) coupled to a modified version of the GEOCARB III model (*17*) (see the Supplementary Materials).

RESULTS

To simulate and reconcile the observed pCO_2 and $\delta^{13}C$ trends during the Cenozoic (Fig. 2, A and B), we include a temperature-dependent mechanism capable of decoupling high production (due to high nutrient concentration) in the surface ocean from high organic carbon export. Temperature exerts two competing effects on organic carbon export and remineralization. On the one hand, higher temperatures elicit increased primary production and stronger carbon export (*18*). On the other hand, high temperatures instigate a higher degradation rate of organic matter sinking through the water column, albeit resulting in a lower amount of organic matter being exported to the ocean floor (*19*). Matsumoto (*20*) quantified the opposing effects that temperature has on the organic carbon pump and, consequently, on pCO_2. The study showed that rising temperatures promote a boost in remineralization at a rate higher than the rise of the export production (the opposite is true for declining temperatures), essentially

School of Ocean and Earth Science and Technology, Department of Oceanography, University of Hawaii 1000 Pope Road, Honolulu, HI 96822, USA.
*Corresponding author. Email: komar@hawaii.edu

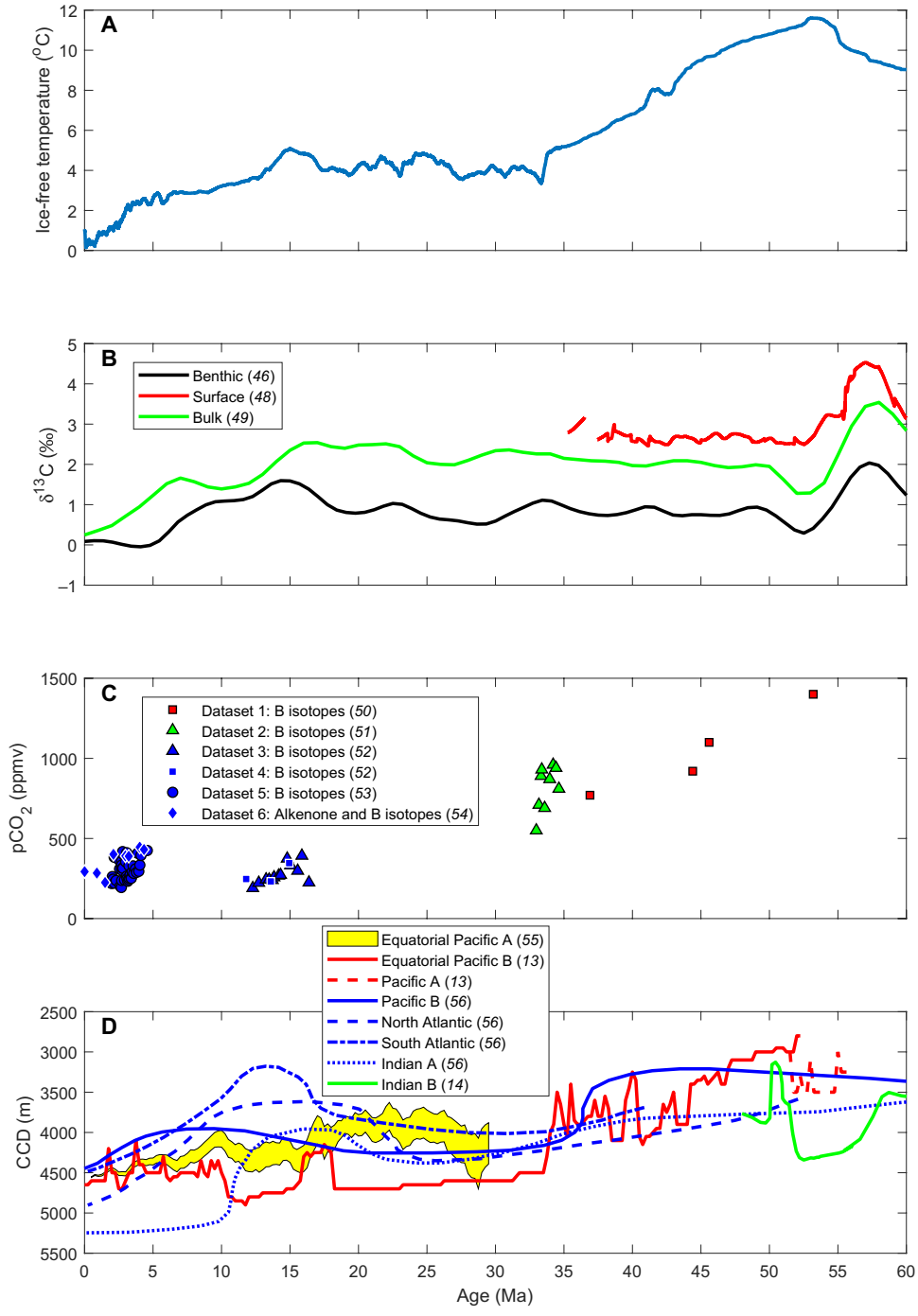

Fig. 1. Compilation of Cenozoic temperature, $\delta^{13}C$, pCO_2, and calcite compensation depth (CCD) history for different ocean basins. (**A**) The reconstructed deep ocean temperature across the Cenozoic is based on the $\delta^{18}O$ data from (*46*). The prescribed temperature change in the model is based on the $\delta^{18}O$-temperature relationship described in (*47*): $T_t = 16.9 - 4.0 \times (\delta^{18}O_t - \delta^{18}O_{sw})$, where $\delta^{18}O_t$ is the observed data and $\delta^{18}O_{sw}$ is the $\delta^{18}O$ of the seawater at a given time in the past (**B**) $\delta^{13}C$ compilation at different depths [benthic, (*46*); surface, (*48*); bulk, (*49*)] and (**C**) atmospheric CO_2 reconstruction based on paleo-proxies from multiple sources: dataset 1 (*50*), dataset 2 (*51*), dataset 3 (*52*), dataset 4 (*52*), dataset 5 (*53*), dataset 6 (*54*), and expressed in parts per million by volume. (**D**) Pacific, Atlantic, and Indian Ocean CCD expressed in meters below sea level. Equatorial Pacific A compiled from (*55*); Equatorial Pacific B and Pacific A from (*13*); Pacific B, North Atlantic, South Athlantic, and Indian A from (*56*); and Indian B from (*14*). Hyperthermals are excluded from the original Indian Ocean CCD data (green line) (*14*).

decoupling export production rates from the organic carbon pump. Hence, it is possible to increase the nutrient supply to surface waters via nutrient redistribution due to higher regeneration rates and higher deep-ocean nutrient inventories while simultaneously decreasing organic carbon burial in the deep ocean. We modeled this behavior by assuming a temperature-dependent Martin curve (see Materials and Methods and the Supplementary Materials). This temperature dependency is critical for reproducing the observed pCO_2 and $\delta^{13}C$

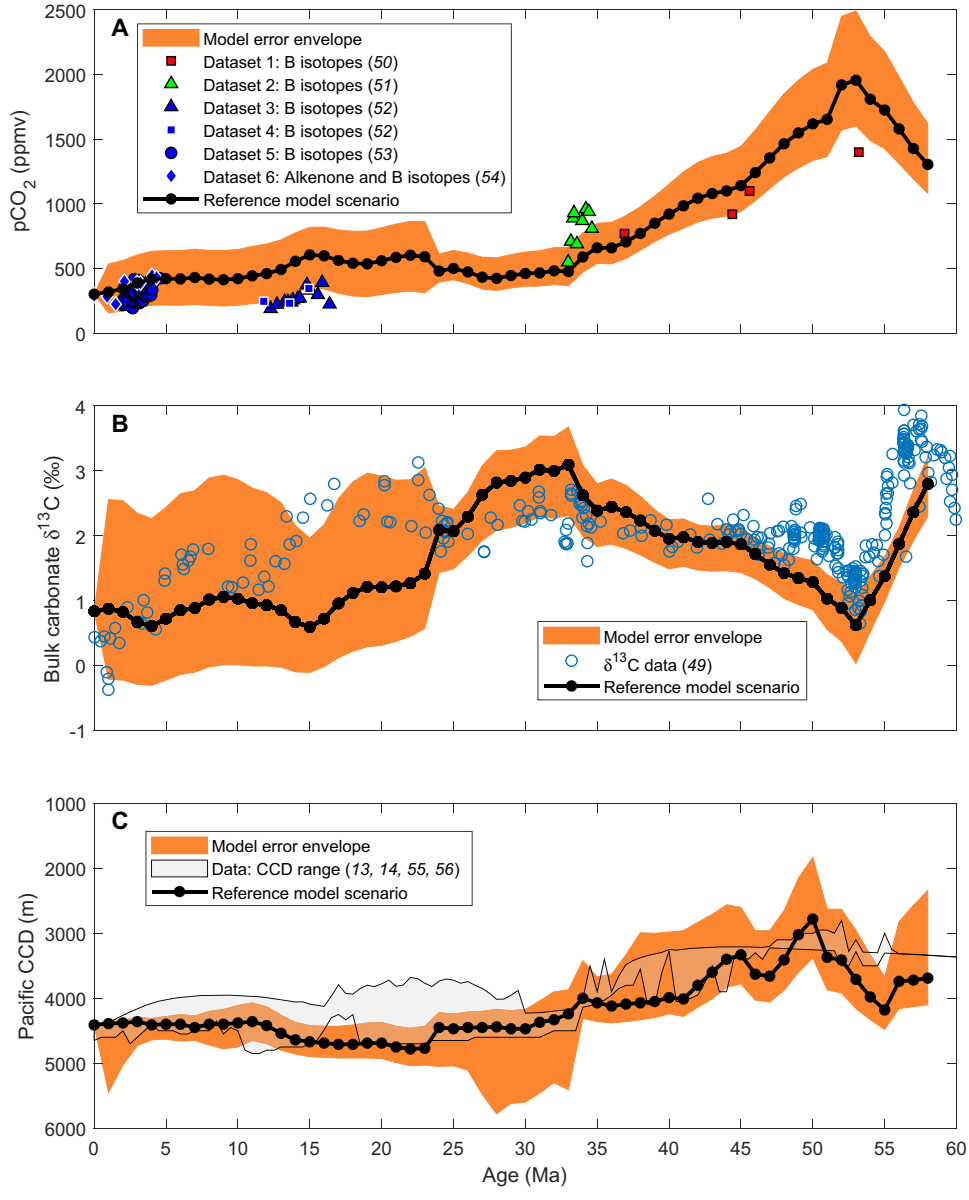

Fig. 2. The reference model simulation (black line with closed black circles) and error envelope (orange area) plotted against the paleo-proxy data displayed and described in Fig. 1. (**A**) Atmospheric pCO_2 predicted by the model in parts per million by volume. (**B**) Model predicted sediment bulk carbonate $\delta^{13}C$ versus the observed sediment data [open blue circles, (*49*)]. ‰, per mil. (**C**) Model predicted evolution of the Pacific CCD against the Pacific CCD data range displayed in Fig. 1. The orange area represents model results for a 95% confidence interval of the Martin curve temperature dependence and the uncertainty associated with the GEOCARB weathering parameters (*57*). The Martin curve temperature dependence is as follows: $b_{(t)} = 0.062 \times T_{(t)} + 0.303(\pm 2\sigma)$, where $b_{(t)}$ is the Martin curve attenuation coefficient at time *t*, and *T* is the median water temperature of the upper 500 m of the water column at time *t*. σ (0.16, calculated in this study) is the SD of residuals (disagreement between the linear regression model and the dataset), and 2σ is the 95% confidence interval.

trends in the model (as illustrated in fig. S18, A and B, when *T* dependency is omitted).

On multimillion year time scales, the continental $CaCO_3$ fluxes must be balanced by the burial of $CaCO_3$ in marine sediments (*11*). Hence, when combined with the $\delta^{13}C$ record and pCO_2 proxies, the CCD provides an additional constraint on global weathering rates and ocean carbonate saturation. There have been a number of studies centered around investigation of the carbon cycle dynamics and climate across the Cenozoic, e.g., (*8*, *17*, *21*–*29*), yet each of the studies is missing one or more critical components of the long-term ocean-atmosphere carbon cycle. For example, (*8*, *17*, *22*–*28*) did not model the CCD; or they modeled the CCD without considering balancing the long-term ocean-atmosphere carbon cycle (*29*). The only previous study modeling the CCD across the entire Cenozoic, which reconciles the weathering fluxes and the CCD trends (albeit lacking a true sediment model), concluded that the changes in sea level and low weatherability of the Paleogene played a major role in controlling the CCD (*21*). In theory, such a scenario allows for decoupling of

weathering rates from the CCD response and permits the multimillion year long periods in which terrestrial weathering steadily declines while the CCD deepens (e.g., during the past ~50 Ma). According to our results, this mechanism may also have played a role in controlling the CCD across this time interval (see below).

To account for the effects of the eustatic sea-level fluctuations in our model, the relative shelf to deep $CaCO_3$ burial was made dependent on the reconstructed sea-level curve (see the Supplementary Materials). Our results indicate that the change in shelf-basin carbonate deposition due to sea-level change is responsible for the overall CCD deepening across the Cenozoic but that the sea-level rise itself is likely not the main mechanism. We propose that latitudinal expansion of carbonate platforms and proliferation of calcifying organisms played a substantial role in controlling the CCD over long time scales.

The peak Cenozoic carbonate mass accumulation rate over the ocean shelf areas (including both shelves and slopes) is observed during the Paleocene and the Eocene (*30*, *31*). The mean rate of carbonate accumulation over the shelves during this time period was about two to three times higher compared to the mean rate during the rest of the Cenozoic (*30*). A larger total Paleogene carbonate accumulation on the shelves is not only attributable to the longitudinal carbonate platform expansion, but it was also a result of the latitudinal expansion of carbonate platforms. While the longitudinal expansion is a result of a higher sea-level stand and a larger shelf area, the latitudinal expansion is a result of the Paleogene extreme warmth (*30*). In the modern ocean, carbonate accumulation is confined between ~30° south and north of the equator, whereas during the early Cenozoic, the carbonate platforms expanded and occupied a wider band around the equator (~45° north and south). A more uniform climate during warm periods, such as during the Late Paleocene and the Early Eocene, likely led to a lower $CaCO_3$ saturation gradient between the poles and the equator, which promoted the latitudinal expansion of carbonate platforms (*30*, *31*).

Coeval with high carbonate accumulation on the shelves was a proliferation (increase in relative species diversity/richness) of the calcifying taxa (coccolithophorids and globigerinina) during the Paleogene (*32*, *33*). The Cenozoic diversity maximum coincides with the warm Paleocene-Eocene epoch, during which the species richness was two to three times higher than during the colder periods (*33*). As the planet cooled during the Late Eocene and into the Oligocene, the species richness exhibited a decline (*33*).

The combination of the Paleocene-Eocene sea-level rise and temperature rise (which peaked around 52 Ma) allowed calcareous organisms to migrate to shallow habitats, expanding the carbonate platforms both longitudinally and latitudinally (*30*, *31*). An expanded shelf area during high sea stands (such as during the LPEE) combined with a larger number of $CaCO_3$-producing organisms over the shelf areas (*33*) [which we postulate was due to increased nutrient supply caused by accelerated weathering and higher phosphate remineralization rates (*34*, *35*)] can accommodate excess alkalinity inputs (caused by higher pCO_2 and temperature). The above-described mechanism largely decouples the CCD from global weathering, resulting in CCD shoaling during the Early Eocene. As the planet cooled and seas regressed following the Eocene climatic optimum, proliferation of calcareous species and migration to the open ocean reversed the above trend and sent the CCD to greater depths (Fig. 2C). We modeled the proliferation and $CaCO_3$ expansion effect by amplifying the shelf-deep $CaCO_3$ partitioning factor (fsh; shelf deposition increase relative to modern) so that the carbonate burial over shelves was ~3 times greater before the Eocene-Oligocene boundary, consistent with the evidence provided above (see the Supplementary Materials).

Our modeling framework demonstrates that the global CCD deepening over the Cenozoic does not necessarily require an increase in global chemical erosion rates, a mechanism often invoked to reconcile the observed trends across this time period (*13*, *36*). Our results are also consistent with the current understanding of the long-term carbon cycling and feedbacks between weathering and atmospheric pCO_2 (*5*). Declining atmospheric CO_2 concentration (*6*), combined with decreasing (or roughly constant) CO_2 degassing rates over the same time period (*8*–*10*), requires a slowdown in (or roughly constant) weathering rates because of the pCO_2-silicate weathering feedback that stabilizes atmospheric CO_2 on geological time scales (*8*). Other mechanisms, such as changes in weatherability, could also have played a role (see Materials and Methods).

The model predicted changes in silicate and carbonate weathering fluxes are also consistent with phosphorus accumulation rates, which appear to be declining between 50 and ~25 Ma (consistent with the total P burial trend in our model; see fig. S17F) (*37*) with notable peaks at around 5 and 15 Ma. However, the long-term Cenozoic decline in phosphorus accumulation rate was interpreted as a contradiction (*37*), because the trend appeared to be in conflict with the Himalayan uplift theory (*36*), which states that the Himalayan orogenesis must have caused an increase in chemical erosion across the Cenozoic. If the weathering rates did not increase during this time interval (see fig. S17), for which there is evidence (*38*), then there is no inconsistency between P accumulation rates and the Cenozoic weathering trends, which further validates our model results.

DISCUSSION

Our results show that including complete ocean carbonate chemistry, prognostic organic carbon/phosphorus burial rates, and $\delta^{13}C$ at various depths, combined with the ability to predict the CCD, is vital for constraining carbon cycle and climate dynamics over multimillion-year time scales. We suggest that metabolic effects caused by elevated temperatures of the Paleogene must be accounted for when the long-term carbon and phosphorus cycles are considered. Otherwise, the predicted organic carbon burial is inconsistent with records of $\delta^{13}C$, temperature, pCO_2, and carbonate accumulation rates. Another fundamental implication from our model outcome is that the observed long-term deepening of the CCD across the Cenozoic does not require an increase in silicate and carbonate weathering fluxes. Our results show that the CCD trends were largely decoupled from silicate and carbonate weathering fluxes during the Cenozoic. We propose that the decoupling developed partially because of the increasing proportion of carbonate buried in the open ocean relative to the shelf carbonate deposition, as the sea level regressed concomitant with global cooling and the formation of continental ice sheets. In addition, combination and interplay of various environmental and physical factors (e.g., temperature, sea-level rise, $CaCO_3$ saturation, nutrient supply and concentration, upwelling, and circulation changes) affected the proliferation and distribution of $CaCO_3$-producing organisms during the Cenozoic.

MATERIALS AND METHODS

All simulations were initiated with modern steady-state fluxes and boundary conditions (see table S1) and with an initial, modern atmospheric CO_2 concentration of 300 parts per million by volume

(ppmv), as provided by GEOCARB. Temperature change in the model is prescribed on the basis of the $\delta^{18}O$ variations rather than being predicted on the basis of the Earth system sensitivity and atmospheric pCO_2 concentration. The rationale behind this approach is that the ocean carbonate chemistry is temperature dependent (obeys highly predictive thermodynamic laws), and we have a continuous and relatively reliable temperature proxy ($\delta^{18}O$) spanning the entire studied interval. In addition, our new modeling framework follows the Arrhenius pattern for chemical reactions, which states that metabolic rates increase with temperature [e.g., (*39*)]. This is implemented in the model as the temperature-dependent remineralization via dynamic particulate organic carbon attenuation factor, which is derived from the empirical data (*40*).

The attenuation of the organic carbon flux in the water column in our model is a function of water depth and is represented by the Martin curve

$$F = F_{z_p} \times \left(\frac{z}{z_p}\right)^{-b} \quad (1)$$

where z_p is the depth of production zones (−100 m) and F_{zp} is the amount of organic carbon exported from the production zone. z is the ocean depth, negative downward (see the Supplementary Materials). b is the coefficient that describes the strength of the decay of the export flux, and its default value is 0.858 (*41*). However, the more recent data question the validity of the Martin curve and propose a wider range of values for b (*42*), which, among other factors, may depend on the ambient water temperature (fig. S5). The Martin curve temperature dependency in this study is modeled after the following equations that describes the dependency of the attenuation factor on temperature (*40*)

$$b_{(t)} = 0.062 \times T_{(t)} + 0.303(\pm 2\sigma) \quad (2)$$

where $b_{(t)}$ is the Martin curve attenuation coefficient at time t, and T is the median water temperature of the upper 500 m of the water column at time t. σ (0.16, calculated in this study) is the SD of residuals (disagreement between the linear regression model and the dataset), and 2σ is the 95% confidence interval. The original formulation of Eq. 2 does not include the SD portion, but it is calculated in this study to produce the model error envelope. To be consistent with the default, modern-day LOSCAR setup, where remineralization rate in the intermediate water (the upper 1000 m) is 78%, the b coefficient at time $t = 0$ (modern) needs to be 0.6737, which requires T of about 6°C. The abovementioned b value is also necessary to produce the modern organic carbon burial rate of 5×10^{12} mol $year^{-1}$ (*17*), which satisfies the preindustrial steady state.

The cumulative organic carbon burial over a depth interval [i.e., intermediate (*m*) and deep ocean (*d*)] is calculated similar to the approach described by Bjerrum *et al.* (*43*); however, our study assumes that organic carbon exported from the surface ocean attenuates according to the Martin curve

$$F_{\mathrm{bg},j} = F_{z_p}(t) \int_{z1}^{z2} \beta(z) \times \frac{dA^*}{dz} \times \left(\frac{z}{z_p}\right)^{-b} dz \quad (3)$$

$$F_{\mathrm{crain},j} = F_{z_p}(t) \int_{z1}^{z2} \frac{dA^*}{dz} \times \left(\frac{z}{z_p}\right)^{-b} dz \quad (4)$$

$$F_{\mathrm{crem},m} = F_{z_p}(t) \times \left(1 - A^* \times \left(\frac{D_t}{z_p}\right)^{-b}\right) - F_{bc,m} \quad (5)$$

$$F_{\mathrm{crem},d} = F_{z_p}(t) - (F_{\mathrm{crem},m} + F_{bc,m} + F_{bc,d}) \quad (6)$$

where $j \in \{m, d\}$, and m and d are intermediate and deep ocean boxes, respectively. F_{bg}, F_{crain}, and F_{crem} are organic carbon burial, organic carbon rain, and organic carbon remineralization, respectively. β is the burial efficiency, which is a function of depth and oxygen (fig. S6). $\frac{dA^*}{dz}$ is the derivative of the normalized hypsographic curve (fig. S6). For organic carbon fluxes (rain, remineralization, and burial) in the intermediate water, z_1 is −1000 m (D_t; table S3) and z_2 is −100 m. z_1 and z_2 for the deep ocean box are −4500 and −1000 m, respectively.

Weatherability estimate

It has been proposed that the silicate weathering flux may have remained relatively constant during the Cenozoic and that the changes in weatherability (*kw*) drove the atmospheric CO_2 concentration (*21*). On the basis of our reference scenario, we carried out a simple calculation estimating the change in weatherability necessary to explain the maximum drop in CO_2 over the Cenozoic. The maximum atmospheric pCO_2 in our reference scenario occurs at 53 Ma (~1960 ppmv), while the lowest is the preindustrial ($t = 0$) CO_2 set to 300 ppmv. Let silicate weathering depend on *kw*, a suite of dimensionless GEOCARB parameters (kGEO for simplicity; see the Supplementary Materials for all parameters), and on atmospheric CO_2

$$F_{\mathrm{Si}} = kw \times \mathrm{kGEO} \times \left(\frac{CO_{2(t)}}{CO_{2(0)}}\right)^{n} \quad (7)$$

where n is the weathering feedback constant set to 0.6 (*15*). As the weatherability scenario assumes no changes in silicate weathering, we set F_{Si} = const. For simplicity, we also keep kGEO constant and ignore carbonate weathering, and then the *kw* at time t reduces to

$$\frac{kw(t)}{kw(0)} = \frac{1}{\left(\frac{CO_{2(t)}}{CO_{2(0)}}\right)^{n}} \quad (8)$$

Therefore, weatherability at $t = 53$ Ma is 0.32, and weatherability at $t = 0$ is 1. It follows that to explain our reference scenario, global weatherability would have to increase by about three times from Early Eocene to present, which is within the range of potential variability (*44*, *45*).

SUPPLEMENTARY MATERIALS

Supplementary material for this article is available at http://advances.sciencemag.org/cgi/content/full/7/4/eabd4876/DC1

REFERENCES AND NOTES

1. J. C. Zachos, M. Pagani, L. Sloan, E. Thomas, K. Billups, Trends, rhythms, and aberrations in global climate 65 Ma to present. *Science* **292**, 686–693 (2001).
2. P. K. Bijl, S. Schouten, A. Sluijs, G. J. Reichart, J. C. Zachos, H. Brinkhuis, Early Palaeogene temperature evolution of the southwest Pacific Ocean. *Nature* **461**, 776–779 (2009).
3. B. S. Cramer, J. R. Toggweiler, J. D. Wright, M. E. Katz, K. G. Miller, Ocean overturning since the Late Cretaceous: Inferences from a new benthic foraminiferal isotope compilation. *Paleoceanogaphy* **24**, PA4216 (2009).
4. N. Komar, R. Zeebe, G. Dickens, Understanding long-term carbon cycle trends: The late Paleocene through the early Eocene. *Paleoceanography* **28**, 650–662 (2013).
5. N. Komar, thesis, University of Hawaii, (2017).
6. D. J. Beerling, D. L. Royer, Convergent cenozoic CO_2 history. *Nat. Geosci.* **4**, 418–420 (2011).

7. Y. G. Zhang, M. Pagani, Z. Liu, S. M. Bohaty, R. DeConto, A 40-million-year history of atmospheric CO_2. *Phil. Trans. R. Soc. A* **371**, 20130096 (2013).
8. R. A. Berner, A. C. Lasaga, R. M. Garrels, The carbonate-silicate geochemical cycle and its effect on atmospheric carbon dioxide over the past 100 million years. *Am. J. Sci.* **283**, 641–683 (1983).
9. R. D. Müller, M. Sdrolias, C. Gaina, B. Steinberger, C. Heine, Long-term sea-level fluctuations driven by ocean basin dynamics. *Science* **319**, 1357 (2008).
10. D. G. Van Der Meer, R. E. Zeebe, D. J. van Hinsbergen, A. Sluijs, W. Spakman, T. H. Torsvik, Plate tectonic controls on atmospheric CO_2 levels since the Triassic. *Proc. Natl. Acad. Sci.* **111**, 4380–4385 (2014).
11. A. Ridgwell, R. E. Zeebe, The role of the global carbonate cycle in the regulation and evolution of the Earth System. *Earth Planet. Sci. Lett.* **234**, 299–315 (2005).
12. T. H. van Andel, T. C. Moore, Cenozoic calcium carbonate distribution and calcite compensation depth in the central equatorial Pacific Ocean. *Geology* **2**, 87 (1974).
13. H. Pälike, W. M. Lyle, H. Nishi, I. Raffi, A. Ridgwell, K. Gamage, A. Klaus, G. Acton, L. Anderson, J. Backman, J. Baldauf, C. Beltran, S. M. Bohaty, P. Bown, W. Busch, J. E. T. Channell, C. O. J. Chun, M. Delaney, P. Dewangan, T. D. Jones, K. M. Edgar, H. Evans, P. Fitch, G. L. Foster, N. Gussone, H. Hasegawa, E. C. Hathorne, H. Hayashi, J. O. Herrle, A. Holbourn, S. Hovan, K. Hyeong, K. Iijima, T. Ito, S.-i. Kamikuri, K. Kimoto, J. Kuroda, L. Leon-Rodriguez, A. Malinverno, T. C. Moore Jr., B. H. Murphy, D. P. Murphy, H. Nakamura, K. Ogane, C. Ohneiser, C. Richter, R. Robinson, E. J. Rohling, O. Romero, K. Sawada, H. Scher, L. Schneider, A. Sluijs, H. Takata, J. Tian, A. Tsujimoto, B. S. Wade, T. Westerhold, R. Wilkens, T. Williams, P. A. Wilson, Y. Yamamoto, S. Yamamoto, T. Yamazaki, R. E. Zeebe, A Cenozoic record of the equatorial Pacific carbonate compensation depth. *Nature* **488**, 609–614 (2012).
14. B. S. Slotnick, V. Lauretano, J. Backman, G. R. Dickens, A. Sluijs, L. Lourens, Early Paleogene variations in the calcite compensation depth: New constraints using old borehole sediments from across Ninetyeast Ridge, central Indian Ocean. *Clim. Past* **11**, 473–493 (2015).
15. R. E. Zeebe, LOSCAR: Long-term Ocean-atmosphere-Sediment CArbon cycle reservoir model v2.0.4. *Geosci. Model Develop.* **1**, 149–166 (2012).
16. N. Komar, R. Zeebe, Redox-controlled carbon and phosphorus burial: A mechanism for enhanced organic carbon sequestration during the petm. *Earth Planet. Sci. Lett.* **479**, 71–82 (2017).
17. R. A. Berner, Z. Kothavala, GEOCARB III: A revised model of atmospheric CO_2 over Phanerozoic time. *Am. J. Sci.* **304**, 397 (2001).
18. R. W. Eppley, Temperature and phytoplankton growth in the sea. *Fish. Bull.* **70**, 1063 (1972).
19. E. A. Laws, P. G. Falkowski, W. O. Smith, H. Ducklow, J. J. McCarthy, Temperature effects on export production in the open ocean. *Global Biogeochem. Cycles* **14**, 1231–1246 (2000).
20. K. Matsumoto, Biology-mediated temperature control on atmospheric pCO2 and ocean biogeochemistry. *Geophys. Res. Lett.* **34**, (2007).
21. L. R. Kump, M. A. Arthur, *Tectonic Uplift and Climate Change* (Springer, 1997), pp. 399–426.
22. L. François, Y. Goddéris, Isotopic constraints on the cenozoic evolution of the carbon cycle. *Chem. Geol.* **145**, 177–212 (1998).
23. K. Wallmann, Controls on the Cretaceous and Cenozoic evolution of seawater composition, atmospheric CO_2 and climate. *Geochim. Cosmochim. Acta* **65**, 3005–3025 (2001).
24. H. Kashiwagi, Y. Ogawa, N. Shikazono, Relationship between weathering, mountain uplift, and climate during the cenozoic as deduced from the global carbon–strontium cycle model. *Palaeogeogr. Palaeoecol.* **270**, 139–149 (2008).
25. R. S. Arvidson, F. T. Mackenzie, M. Guidry, Magic: A Phanerozoic model for the geochemical cycling of major rock-forming components. *Am. J. Sci.* **306**, 135–190 (2006).
26. G. Li, J. Ji, J. Chen, D. B. Kemp, Evolution of the Cenozoic carbon cycle: The roles of tectonics and CO_2 fertilization. *Global Biogeochem. Cycles* **23**, GB1009 (2009).
27. G. Li, H. Elderfield, Evolution of carbon cycle over the past 100 million years. *Geochim. Cosmochim. Acta* **103**, 11–25 (2013).
28. J. K. Caves, A. B. Jost, K. V. Lau, K. Maher, Cenozoic carbon cycle imbalances and a variable weathering feedback. *Earth Planet. Sci. Lett.* **450**, 152–163 (2016).
29. R. van der Ploeg, B. P. Boudreau, J. J. Middelburg, A. Sluijs, Cenozoic carbonate burial along continental margins. *Geology* **47**, 1025–1028 (2019).
30. B. N. Opdyke, B. H. Wilkinson, Surface area control of shallow cratonic to deep marine carbonate accumulation. *Paleoceanography* **3**, 685–703 (1988).
31. S. K. Boss, B. H. Wilkinson, Planktogenic/eustatic control on cratonic/oceanic carbonate accumulation. *J. Geol.* **99**, 497–513 (1991).
32. R. E. Martin, Cyclic and secular variation in microfossil biomineralization: Clues to the biogeochemical evolution of Phanerozoic oceans. *Global Planet. Change* **11**, 1–23 (1995).
33. P. R. Bown, J. A. Lees, J. R. Young, *Coccolithophores* (Springer, 2004), pp. 481–508.
34. P. W. Homewood, The carbonate feedback system; interaction between stratigraphic accomodation, ecological succession and the carbonate factory. *Bull. Soc. Géol. Fr.* **167**, 701–715 (1996).
35. J. Masse, L. Montaggioni, Growth history of shallow-water carbonates: Control of accommodation on ecological and depositional processes. *Inl. J. Earth Sci.* **90**, 452–469 (2001).
36. M. E. Raymo, W. F. Ruddiman, Tectonic forcing of late Cenozoic climate. *Nature* **359**, 117–122 (1992).
37. M. L. Delaney, G. M. Filippelli, An apparent contradiction in the role of phosphorus in Cenozoic chemical mass balances for the world ocean. *Paleoceanography* **9**, 513–527 (1994).
38. J. K. Willenbring, F. von Blanckenburg, Long-term stability of global erosion rates and weathering during late-Cenozoic cooling. *Nature* **465**, 211–214 (2010).
39. S. M. Stanley, Relation of Phanerozoic stable isotope excursions to climate, bacterial metabolism, and major extinctions. *Proc. Natl. Acad. Sci. U.S.A.* **107**, 19185–19189 (2010).
40. C. M. Marsay, R. J. Sanders, S. A. Henson, K. Pabortsava, E. P. Achterberg, R. S. Lampitt, Attenuation of sinking particulate organic carbon flux through the mesopelagic ocean. *Proc. Natl. Acad. Sci. U.S.A.* **112**, 1089–1094 (2015).
41. J. H. Martin, G. A. Knauer, D. M. Karl, W. W. Broenkow, VERTEX: Carbon cycling in the northeast Pacific. *Deep Sea Res.* **34**, 267–285 (1987).
42. K. O. Buesseler, C. H. Lamborg, P. W. Boyd, P. J. Lam, T. W. Trull, R. R. Bidigare, J. K. B. Bishop, K. L. Casciotti, F. Dehairs, Frank, M. Elskens, M. Honda, D. M. Karl, D. A. Siegel, M. W. Silver, D. K. Steinberg, J. Valdes, B. Van Mooy, S. Wilson, Revisiting carbon flux through the ocean's twilight zone. *Science* **316**, 567 (2007).
43. C. J. Bjerrum, J. Bendtsen, J. J. F. Legarth, Modeling organic carbon burial during sea level rise with reference to the Cretaceous. *Geochem. Geophys. Geosyst.* **7**, Q05008 (2006).
44. S. Misra, P. N. Froelich, Lithium isotope history of Cenozoic seawater: Changes in silicate weathering and reverse weathering. *Science* **335**, 818–823 (2012).
45. L. R. Kump, Prolonged Late Permian–Early Triassic hyperthermal: Failure of climate regulation? *Philos. Trans. R. Soc. A* **376**, 20170078 (2018).
46. J. C. Zachos, G. R. Dickens, R. E. Zeebe, An early Cenozoic perspective on greenhouse warming and carbon-cycle dynamics. *Nature* **451**, 279–283 (2008).
47. B. E. Bemis, H. J. Spero, J. Bijma, D. W. Lea, Reevaluation of the oxygen isotopic composition of planktonic foraminifera: Experimental results and revised paleotemperature equations. *Paleoceanography* **13**, 150–160 (1998).
48. A. K. Hilting, L. R. Kump, T. J. Bralower, Variations in the oceanic vertical carbon isotope gradient and their implications for the Paleoce-Eocene biological pump. *Paleoceanography* **23**, PA3222 (2008).
49. A. Kurtz, L. R. Kump, M. A. Arthur, J. C. Zachos, A. Paytan, Early Cenozoic decoupling of the global carbon and sulfur cycles. *Paleoceanogr. Paleoclimatol.* **18**, 1090 (2003).
50. E. Anagnostou, E. H. John, K. M. Edgar, G. L. Foster, A. Ridgwell, G. N. Inglis, R. D. Pancost, D. J. Lunt, P. N. Pearson, Changing atmospheric CO_2 concentration was the primary driver of early Cenozoic climate. *Nature* **533**, 380 (2016).
51. P. N. Pearson, G. L. Foster, B. S. Wade, Atmospheric carbon dioxide through the eocene-oligocene climate transition. *Nature* **461**, 1110–1113 (2009).
52. G. L. Foster, C. H. Lear, J. W. Rae, The evolution of pCO_2, ice volume and climate during the middle Miocene. *Earth Planet. Sci. Lett.* **341**, 243 (2012).
53. G. Bartoli, B. Hönisch, R. E. Zeebe, Atmospheric CO2 decline during the Pliocene intensification of northern hemisphere glaciations. *Paleoceanography* **26**, PA4213 (2011).
54. O. Seki, G. L. Foster, D. N. Schmidt, A. Mackensen, K. Kawamura, R. D. Pancost, Alkenone and boron-based pliocene pCO_2 records. *Earth Planet. Sci. Lett.* **292**, 201–211 (2010).
55. S. M. Campbell, R. Moucha, L. A. Derry, M. E. Raymo, Effects of dynamic topography on the cenozoic carbonate compensation depth. *Geochem. Geophys. Geosyst.* **19**, 1025 (2018).
56. T. H. van Andel, Mesozoic/Cenozoic calcite compensation depth and the global distribution of calcareous sediments. *Earth Planet. Sci. Lett.* **26**, 187–194 (1975).
57. D. L. Royer, Y. Donnadieu, J. Park, J. Kowalczyk, Y. Goddéris, Error analysis of CO_2 and O_2 estimates from the long-term geochemical model GEOCARBSULF. *Am. J. Sci.* **314**, 1259–1283 (2014).
58. R. E. Zeebe, D. A. Wolf-Gladrow, *CO_2 in Seawater: Equilibrium, Kinetics, Isotopes* (Elsevier Oceanography Series, 2001), pp. 346.
59. J. Veizer, D. Ala, K. Azmy, O. Bruckschen, D. Buhl, F. Bruhn, G. A. F. Carden, A. Diener, S. Ebneth, Y. Goddéris, T. Jasper, C. Korte, C. F. Pawellek, O. G. Podlaha, H. Strauss, $^{87}Sr/^{86}Sr$, $\delta^{13}C$ and $\delta^{18}O$ evolution of Phanerozoic seawater. *Chem. Geol.* **161**, 59–88 (1999).
60. T. Westerhold, U. Rohl, B. Donner, H. K. McCarren, J. C. Zachos, A complete high-resolution Paleocene benthic stable isotope record for the central Pacific (ODP Site 1209). *Paleoceanography* **26**, PA2216 (2011).
61. G. R. Dickens, J. Backman, Core alignment and composite depth scale for the lower Paleogene through uppermost Cretaceous interval at Deep Sea Drilling Project Site 577. *Newslett. Stratigraphy* **46**, 47–68 (2013).

62. R. Samworth, H. Poore, Understanding past ocean circulations: A nonparametric regression case study. *Stat. Model.* **5**, 289 (2005).
63. H. Poore, R. Samworth, N. White, S. Jones, I. McCave, Neogene overflow of northern component water at the greenland-scotland ridge. *Geochem. Geophys. Geosyst.* **7**, Q06010 (2006).
64. T. Tyrrell, The relative influences of nitrogen and phosphorus on oceanic primary production. *Nature* **400**, 525–531 (1999).
65. J. L. Sarmiento, N. Gruber, *Ocean Biogeochemical Dynamics: Princeton* (Princeton Univ. Press, 2006).
66. P. Van Cappellen, E. D. Ingall, Redox stabilization of the atmosphere and oceans by phosphorus-limited marine productivity. *Science* **271**, 493 (1996).
67. L. R. Kump, S. L. Brantley, M. A. Arthur, Chemical weathering, atmospheric CO_2, and climate. *Annu. Rev. Earth Planet. Sci.* **28**, 611–667 (2000).
68. S. Flögel, K. Wallmann, C. J. Poulsen, J. Zhou, A. Oschlies, S. Voigt, W. Kuhnt, Simulating the biogeochemical effects of volcanic CO_2 degassing on the oxygen-state of the deep ocean during the cenomanian/turonian anoxic event (OAE2). *Earth Planet. Sci. Lett.* **305**, 371–384 (2011).
69. T. Tyrrell, R. E. Zeebe, History of carbonate ion concentration over the last 100 million years. *Geochim. Cosmochim. Acta* **68**, 3521 (2004).
70. H. W. Menard, S. M. Smith, Hypsometry of ocean basin provinces. *J. Geophys. Res.* **71**, 4305 (1966).
71. K. L. Bice, E. J. Barron, W. H. Peterson, *Tectonic Boundary Conditions for Climate Reconstructions*, T. J. Crowley, K. C. Burke, Eds. (Oxford Univ. Press, 1998), pp. 227–247.
72. N. Herold, M. Seton, R. D. Müller, Y. You, M. Huber, Middle Miocene tectonic boundary conditions for use in climate models. *Geochem. Geophys. Geosyst.* **9**, Q10009 (2008).
73. M. F. Stuecker, thesis, Carl-von-Ossietzky Universität Oldenburg, Germany (2009).
74. M. F. Stuecker, R. E. Zeebe, Ocean chemistry and atmospheric CO2 sensitivity to carbon perturbations throughout the cenozoic. *Geophys. Res. Lett.* **37**, L03609 (2010).
75. J. R. Toggweiler, Variation of atmospheric CO_2 by ventilation of the ocean's deepest water. *Paleoceanography* **14**, 571–588 (1999).
76. C. Slomp, P. Van Cappellen, The global marine phosphorus cycle: Sensitivity to oceanic circulation. *Biogeosciences* **4**, 155–171 (2007).
77. I. Tsandev, C. Slomp, Modeling phosphorus cycling and carbon burial during cretaceous oceanic anoxic events. *Earth Planet. Sci. Lett.* **286**, 71–79 (2009).
78. K. Wallmann, Feedbacks between oceanic redox states and marine productivity: A model perspective focused on benthic phosphorus cycling. *Global Biogeochem. Cycles* **17**, 1084 (2003).
79. R. A. Berner, GEOCARB II: A revised model of atmospheric CO_2 over Phanerozoic time. *Am. J. Sci.* **294**, 56–91 (1994).
80. M. Iversen, H. Ploug, Temperature effects on carbon-specific respiration rate and sinking velocity of diatom aggregates–potential implications for deep ocean export processes. *Biogeosciences* **10**, 4073–4085 (2013).
81. T. K. Lowenstein, R. V. Demicco, Elevated eocene atmospheric CO_2 and its subsequent decline. *Science* **313**, 1928 (2006).
82. M. A. Kominz, J. V. Browning, K. G. Miller, P. J. Sugarman, S. Mizintseva, C. R. Scotese, Late Cretaceous to Miocene sea-level estimates from the New Jersey and Delaware coastal plain coreholes: An error analysis. *Basin Res.* **20**, 211–226 (2008).
83. M. Raitzsch, B. Hönisch, Cenozoic boron isotope variations in benthic foraminifers. *Geology* **41**, 591–594 (2013).

Acknowledgments: We thank the editor D. Lea, L. Kump, and one anonymous reviewer for comments and suggestions that improved the manuscript. **Funding:** This work was supported by NSF grant OCE16-58023 to R.E.Z. **Author contributions:** N.K. wrote the manuscript and expanded and modified the LOSCAR model originally developed by R.E.Z. R.E.Z. provided guidance during model development and contributed to refining the manuscript text. **Competing interests:** The authors declare that they have no competing interests. **Data and materials availability:** All data needed to evaluate the conclusions in the paper are present in the paper and/or the Supplementary Materials. Additional data related to this paper may be requested from the authors.

Submitted 24 June 2020
Accepted 3 December 2020
Published 22 January 2021
10.1126/sciadv.abd4876

Citation: N. Komar, R. E. Zeebe, Reconciling atmospheric CO_2, weathering, and calcite compensation depth across the Cenozoic. *Sci. Adv.* **7**, eabd4876 (2021).

Science Advances

Reconciling atmospheric CO_2, weathering, and calcite compensation depth across the Cenozoic

Nemanja Komar and Richard E. Zeebe

Sci Adv **7** (4), eabd4876.
DOI: 10.1126/sciadv.abd4876

Science Advances (ISSN 2375-2548) is published by the American Association for the Advancement of Science, 1200 New York Avenue NW, Washington, DC 20005. The title *Science Advances* is a registered trademark of AAAS.